# Quantitative High-Throughput Screening of Osteoblast Attachment, Spreading, and Proliferation on Demixed Polymer Blend Micropatterns

Pedro Zapata,[†] Jing Su,[‡] Andrés J. García,[§] and J. Carson Meredith*,[†]

*School of Chemical and Biomolecular Engineering, Coulter School of Biomedical Engineering, and Woodruff School of Mechanical Engineering, Georgia Institute of Technology, Atlanta, Georgia*

*Received November 30, 2006; Revised Manuscript Received February 21, 2007*

Designing materials that regulate cell function in a desired manner is a major goal of biomaterials engineering. Challenges include the vast material property space to be explored, the complexity of cell−surface interactions, and the empirical nature of research in this field. To address these challenges, combinatorial methods have been developed in recent years for screening cell responses to material surfaces. Previous work using gradient libraries of biodegradable polymers poly(ϵ-caprolactone) and poly(D,L-lactide) showed qualitatively that alkaline phosphatase activity of MC3T3-E1 osteoblasts was dramatically enhanced at specific blend compositions and temperatures. In this study, we expand the combinatorial screening to measure quantitatively early events in the osteoblast life cycle: attachment, spreading, and proliferation. In addition, this work relates these cell assays to quantitative measures of polymer surface microstructure and topography. In general, cell attachment was favored on the more hydrophilic PDLA domains. However, cell spreading was strongly influenced by phase-separated microstructures on the polymer surfaces. Regions of enhanced cell proliferation shifted from one microstructural region to others as the culture progressed from 3 to 8 days. Viability showed no response to the surface features of the libraries. These screening results indicate the precise preparatory conditions and microstructure/topography ranges that should be used to design future confirmatory studies of the fundamental mechanisms of cell response to these heterogeneous patterned surfaces. Given the complex nature and breadth of these parameters, the simplification of the parameter space to be explored is an important advance.

## 1. Introduction

The interaction of cells with materials is exceptionally complicated, and its study is of great relevance in the development of functional biomaterials for use in tissue engineering and biomedicine. Surface chemistry is a crucial aspect in determining the degree of biocompatibility of a particular material.[1] In fact, surface chemical groups of synthetic materials have strong effects on focal adhesion, intracellular signaling events, and cell function.[2−6] Modifying material surface chemistry with grafted functional groups,[7] immobilized peptides,[8,9] and other approaches[10,11] are effective ways to improve biocompatibility and influence cell behavior. Similarly, surface physical patterning and microtopography exert significant influence on attachment-dependent cells, being able to modulate cell shape and cytoskeletal tension,[12−14] which in turn impact cell attachment, migration,[15] cellular orientation,[16] proliferation, and protein expression.[17−19]

Ideally, biomaterials would display a combination of physical and chemical surface characteristics designed specifically to regulate cell behavior in a desired manner. One class of materials that shows promise in this regard is demixed polymer blends,[20−22] which phase separate as a function of composition and temperature to produce chemically distinct nano- and micropatterns. Various cell types have been shown to respond to changes in the size, shape, and chemistry of these nano- and microstructural features.[20−22] Polymer blends may offer opportunities for patterning the internal surfaces of complex three-dimensional tissue engineering constructs, which is a limitation of lithographic patterning methods. Challenges to finding a polymer blend with the optimum combination of chemical and physical surface properties include the vast number of compositional and experimental variables involved and the complexity and noise inherent to cell-based assays. These challenges hinder development of new biomaterials based on the demixing concept. The recent emergence of combinatorial sample design and preparation, coupled with high-throughput screening techniques, in polymer and materials science offers opportunities to streamline the characterization of complex material-dependent cell responses.[23−35] These techniques provide a suitable framework to address the large variable space[7,36] and sensitivity to environmental effects. In complex, multivariate systems, primary screening (high throughput, low accuracy) is used in order to "discover" parameters where hypotheses can be tested optimally in secondary (low throughput, high accuracy) experiments.

Poly(ϵ-caprolactone) (PCL) and poly(D,L-lactide) (PDLA), broadly used in FDA-approved biodegradable devices, hold contrasting material properties (i.e., crystallinity, glass transition temperature, degradation rate, and tensile modulus)[37] that make them excellent candidates for the development of materials that explore a wider range of physicochemical properties and biological interactions than homogeneous polymers. Yet, few studies have examined the cell responses to mixtures of these and similar materials.[38] PCL/PDLA blends exhibit lower critical solution temperature (LCST) phase behavior[39] that in conjunction with PCL crystallization generates temperature- and composition-dependent phase-separated microstructures. Combinatorial libraries[26,40,41] have been prepared using *continuous*

[†] School of Chemical and Biomolecular Engineering.
[‡] Coulter School of Biomedical Engineering.
[§] Woodruff School of Mechanical Engineering.

10.1021/bm061134t CCC: $37.00 
Published on Web 05/17/2007

composition and annealing temperature gradients that create diverse surface morphologies across the libraries, allowing concurrent evaluation of the effect of hundreds of dissimilar surface characteristics on cell function. The potential of this approach was shown in previous work in which specific combinations of composition and process temperature produced an amplification of alkaline phosphatase (ALP) production in MC3T3-E1 osteoblast-like cells.[26] While promising, this previous work utilized only a qualitative assay of protein expression and did not explore other cell events that occur prior to ALP expression. Here, we examine other key developmental stages of MC3T3-E1 osteoblasts, including attachment, spreading, and proliferation on PCL/PDLA. The purpose of this primary screening study is to discover the "active" regions of parameter (temperature, composition) space that have the strongest effects on early cell events. In so doing, we demonstrate the use of quantitative immunofluorescence assays at a high density of points on the combinatorial libraries. The value of this study is the discovery of parameter sets that will be used to design future experiments that seek cause-and-effect relationships between demixed microstructure and cell response.

## 2. Materials and Methods

**2.1. Preparation of Combinatorial Libraries.** PCL/PDLA combinatorial libraries with linear composition gradients were prepared from identical mass fraction solutions ($X = 0.05$) of PDLA (Alkermes Medisorb 100DL high I.V. poly(D,L-lactide), $M_w = 127\,000$, $M_w/M_n = 1.56$, lot no. 0103-442) and PCL (Aldrich Chemical Co., $M_n = 80\,000$, $M_w/M_n = 1.425$, lot no. 07526HI) dissolved in chloroform (EM science, ACS grade), using a gradient-film coating technique.[41,42] The libraries were prepared on 24 mm × 24 mm silicon <100> chips (Silicon, Inc.), previously etched in 6:1 buffered oxide etch ($HF/NHF_4$, J.T. Baker) to create a hydrophobic surface and avoid polymer delamination throughout the cell culture period. Diverse surface morphological lateral patterns were obtained inducing PCL/PDLA LCST[39] phase separation by annealing the libraries for 2 h over a linear temperature gradient[40] orthogonal to the composition gradient. Finished libraries presented orthogonal composition and process temperature gradients ranging from $0.18 < \phi_{PDLA} < 1$ and 76.3 °C < $T$ < 120 °C, respectively. Approximately 82 libraries were used in the course of this study, including samples for both physical characterization tests and bioassays.

**2.2. Characterization of Combinatorial Libraries.** *2.2.1. Ellipsometry.* Thickness of combinatorial libraries was measured with a wide spectral range V-VASE variable angle spectroscopic ellipsometer (J.A. Woollam Co.). Optical constants and film thickness were obtained executing a point-to-point data fitting on the transparent Cauchy region ($700 < \lambda < 1100$ nm) (WVASE32, J.A. Woollam Co.). Thickness values were determined by several iterations using the Marquardt−Levenberg algorithm.

*2.2.2. Fourier Transform Infrared Spectroscopy (FTIR).* Absorption spectra were collected with an IRscope II (Bruker Optics Inc.) using a KBr beam splitter at room temperature. Spectra were measured and averaged 128 times at a resolution of 4 $cm^{-1}$ for several locations of distinct composition over the library. Bands in the $CH_3$ asymmetric/symmetric stretch region ($\nu = 2970-2950/2880-2860$ $cm^{-1}$) and the $CH_2$ asymmetric/symmetric stretch region ($\nu = 2935-2915/2865-2845$ $cm^{-1}$) were resolved using Peakfit (Systat Soft Inc.) peak separation and analysis software. Deconvolution and fitting to obtain the area of the IR absorption peaks in the aforementioned regions was carried out using Peakfit's Gaussian amplitude IRF deconvolution procedure following a spectrum baseline subtraction via a zero second-derivative algorithm. Ratios of these areas and the areas of equivalent peaks of PCL/PDLA polymer standards of known composition (25%, 50%, 75%, and 100% PCL) were used to determine the approximate composition of different spots over the library.

*2.2.3. Atomic Force Microcopy (AFM).* Surface topography characterization was performed with an Explorer scanning probe microscope (SPM) (Veeco Instruments Inc.) using a gold-coated silicon nitride V-shaped cantilever (part no. MLCT-EXMT-A, Veeco metrology group). Data was acquired in contact and force modulation modes over 36 distinct locations along the libraries. Sampling area and scanning rate were 100 μm × 100 μm and 200 μm/s, respectively. Surface structure of different spots of annealed PCL/PDLA libraries was visualized from the *z*-modulation maps (force modulation mode), while average microdomain height and root-mean-square roughness were determined from the topography maps (standard air contact mode).

*2.2.4. Cross-Polarized Optical Microscopy.* Surface structure visualization was conducted using an automated BX51 cross-polarized microscope (Olympus Corp.). Polarizer filters were operated at a high extinction factor to achieve high contrast between the glassy amorphous PDLA phase and the crystalline PCL phase. Images were corrected (i.e., shading and contrast equalization), processed (i.e., thresholding and binary filtering), and analyzed using ImageJ (NIH, public domain) and SigmaScan Pro (Systat software Inc.) for microdomain size characterization, expressed as particle maximal Feret's diameter ($F_{max}$). We evaluated 36 locations per library, matching those scanned using AFM.

*2.2.5. Static Contact Angle.* Surface wettability was measured with a Rame-Hart 100 goniometer using the sessile drop method for static contact angles. Images of deionized water drops (approximately 2−3 μL) placed over the library surface were analyzed using ImageJ (NIH, public domain) to account for contact angle values.

**2.3. Cell Harvesting and Culturing.** Murine MC3T3-E1 cells were acquired from the RIKEN Bioresource Center Cell Bank (Ibaraki, Japan). Established from newborn mouse calvaria,[43] the MC3T3-E1 cell line has been shown capable of differentiating into osteoblast and osteocytes in vitro.[44] MC3T3-E1 cells have been shown to exhibit specific bone-related protein expression patterns, under different developmental stages, similar to mouse calvaria primary cells.[44,45] This cell line is a good in vitro model for investigating cell behaviors, regulations of such behaviors, and underlying mechanisms of early stages of osteoblast maturation.[46] Cells were cultured in alpha minimum essential medium (α-MEM) (Invitrogen Corp.) supplemented with 10% fetal bovine serum (FBS) (Hyclone) and 1% penicillin−streptomycin (Invitrogen Corp.). Prior to seeding cells were washed with $Ca^{2+}$- and $Mg^{2+}$-free phosphate-buffered saline DPBS (1×) (Invitrogen Corp.) and detached via trypsinization (0.05% trypsin, 0.53 mM EDTA·4Na; Invitrogen Corp.). Cell viability was >95% based on trypan blue exclusion. Libraries were sterilized by immersion in a 70% ethanol−30% water solution for 10 min and placed in Costar six-well ultralow attachment microplates (Corning, Inc.). Cells, passages 4−7, were seeded on the libraries at a low density of 5000 cells/$cm^2$ in α-MEM supplemented with 10% FBS and 1% penicillin−streptomycin. Cell culture media was exchanged every other day. Starting at day 3 in culture, osteogenic supplements (50 μg/mL L-ascorbic acid (Sigma-Aldrich, Inc.) and 3 mM Na-β-glycerophosphate (Sigma-Aldrich, Inc.) were added to the cell culture media. Cells were cultured at identical conditions on tissue culture polystyrene (TCPS) dishes as a uniform surface control.

**2.4. Cell Adhesion and Spreading (Morphology).** Initial cell attachment and spreading at 6 h was determined via immunofluorescence labeling of cytoskeleton F-actin fibers and the focal adhesion component vinculin as previously described.[47] Cold cytoskeleton buffer (50 mM NaCl, 150 mM sucrose, 3 mM $MgCl_2 \cdot 6H_2O$, 50 mM Tris, pH 6.8) supplemented with 0.5% Triton X-100 (IBI/Shelton Scientific) and protease inhibitors (20 μg/mL aprotinin, 1 μg/mL leupeptin (Sigma-Aldrich, Inc.), 2 mM phenylmethylsulfonylfluoride (EM Science)) was added for cell permeabilization, followed by fixation in 3.6% (v/v) formaldehyde (4 °C). Cells were incubated in mouse antivinculin antibody (Upstate Group Inc.), rinsed, and incubated in AlexaFluor488-conjugated goat antimouse IgG (Molecular Probes, Inc.) and rhodamine-conjugated phalloidin (Molecular Probes, Inc.). Cell nuclei were

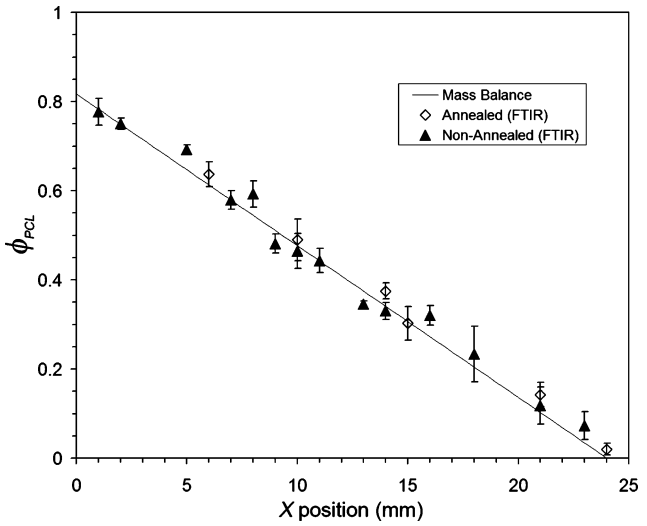


**Figure 1.** PCL mass fraction vs position over a PCL/PDLA library. The solid line represents the expected PCL mass fraction (mass balance). Markers represent the average value of the PCL concentration calculated at the same location in two separate libraries (closed triangles: nonannealed libraries. Open diamonds: libraries annealed for 2 h at 100 °C). Standard uncertainty given by error bars (±SEM, $n = 2$ replicates).

counterstained with Hoechst (Molecular Probes, Inc.) and used to quantify cell density. Cells were visualized using a Nikon Eclipse E400 fluorescence microscope (Nikon Corp.) coupled with a SPOT RT slider camera (Diagnostic Instruments, Inc.). The following dilutions of stock antibodies in PBS were utilized: antivinculin IgG 1:500, rhodamine-conjugated phalloidin 1:200, AlexaFluor488-conjugated antimouse IgG 1:200, and Hoechst 1:10 000.

Cell morphology was assessed via image analysis using a custom adaptive edge detection procedure developed with ImageJ. Following background subtraction from negative control libraries and image equalization images were converted to grayscale. The procedure automatically iterates through different threshold values (binary images) for image segmentation using a "chessboard" distance transform $d_{\text{chessboard}}([k_1, j_1],[k_2, j_2]) = \max(|k_1 - k_2|,|j_1 - j_2|)$, where $d_{\text{chessboard}}([k_1, j_1],[k_2, j_2])$ is the distance between two pixels $[k_1, j_1]$ and $[k_2, j_2]$. Watershed segmented areas are divided in variable size grids, and a Sobel detector is used to approximate derivatives to find the maximum gradient along the grid's edges or pixel neighborhoods, corresponding to the intersections of the cell boundary and the grid. Cell boundaries were formed by a sequence of linear segments of contiguous local maxima points. Morphology was quantified by a cell circularity factor $C$ defined as $4\pi(A/P^2)$, where $A$ and $P$ are the cell area and perimeter, respectively.

**2.5. Cell Proliferation.** Cell proliferation was assayed by immunostaining of BrdU (a thymidine analog) incorporated during DNA replication. BrdU (Sigma-Aldrich, Inc.) (10 $\mu$g/mL) was added to the cell culture medium 6 h prior to cell fixation. Cells were treated with ice-cold 2 N HCl for 20 min and washed three times with 100 mM TRIS-50 mM NaCl (pH 7.6). Following washing in DPBS and blocking in 5% goat serum, cultures were incubated in monoclonal anti-BrdU (clone BU 33, Sigma-Aldrich, Inc.) and AlexaFluor488-conjugated goat antimouse IgG antibodies. Cell nuclei were counterstained with ethidium homodimer-2 (Molecular Probes, Inc.). Cultures were scored by fluorescence microscopy for proliferation as the ratio of cells positive for BrdU incorporation relative to cell nuclei. Cell proliferation was monitored on separate libraries at 3, 4, 5, 8, and 13 days after the initial culture time.

**2.6. Cell Viability.** Cell viability was evaluated measuring intracellular esterase activity and plasma membrane integrity via a two-color fluorescence LIVE/DEAD Viability/Cytotoxicity assay kit (Molecular

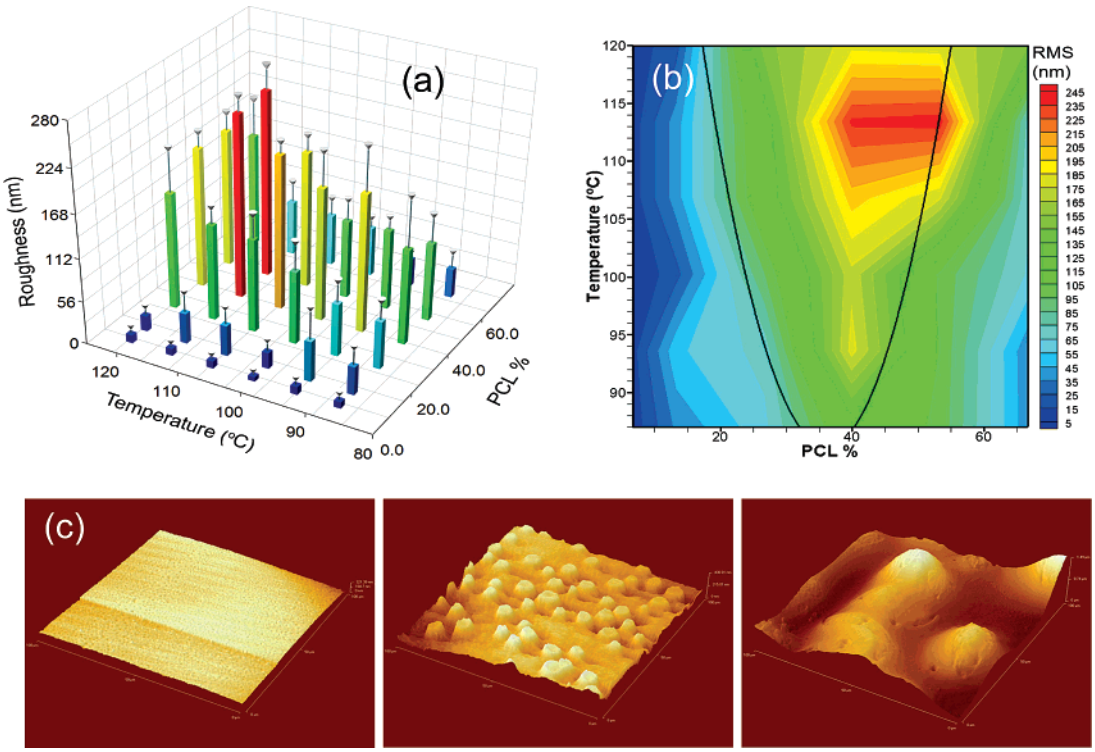


**Figure 2.** Library surface roughness characterization. (a) Root-mean-square surface roughness profile of an annealed PCL/PDLA composition-gradient library. Values presented as averages ± SEM (indicated by error bars delimited with inverted cone markers, $n = 3$ replicates). (b) Average root-mean-square surface roughness contour map over the library. The solid "U-shaped" line indicates the boundary of the LCST regime. (c) Three-dimensional extensions of AFM topography maps representing the surface microstructure of various locations of the PCL/PDLA libraries (scanned area: 100 $\mu$m × 100 $\mu$m): 10%PCL/90%PDLA 95 °C, nonsegregated continuous morphology (left), 26%PCL/74%PDLA 120 °C, discrete PCL-rich droplet-like domains dispersed in a continuous PDLA-rich matrix (middle), 53%PCL/47%PDLA 120 °C, merged PCL-rich domains forming a bicontinuous PCL/PDLA matrix (right).

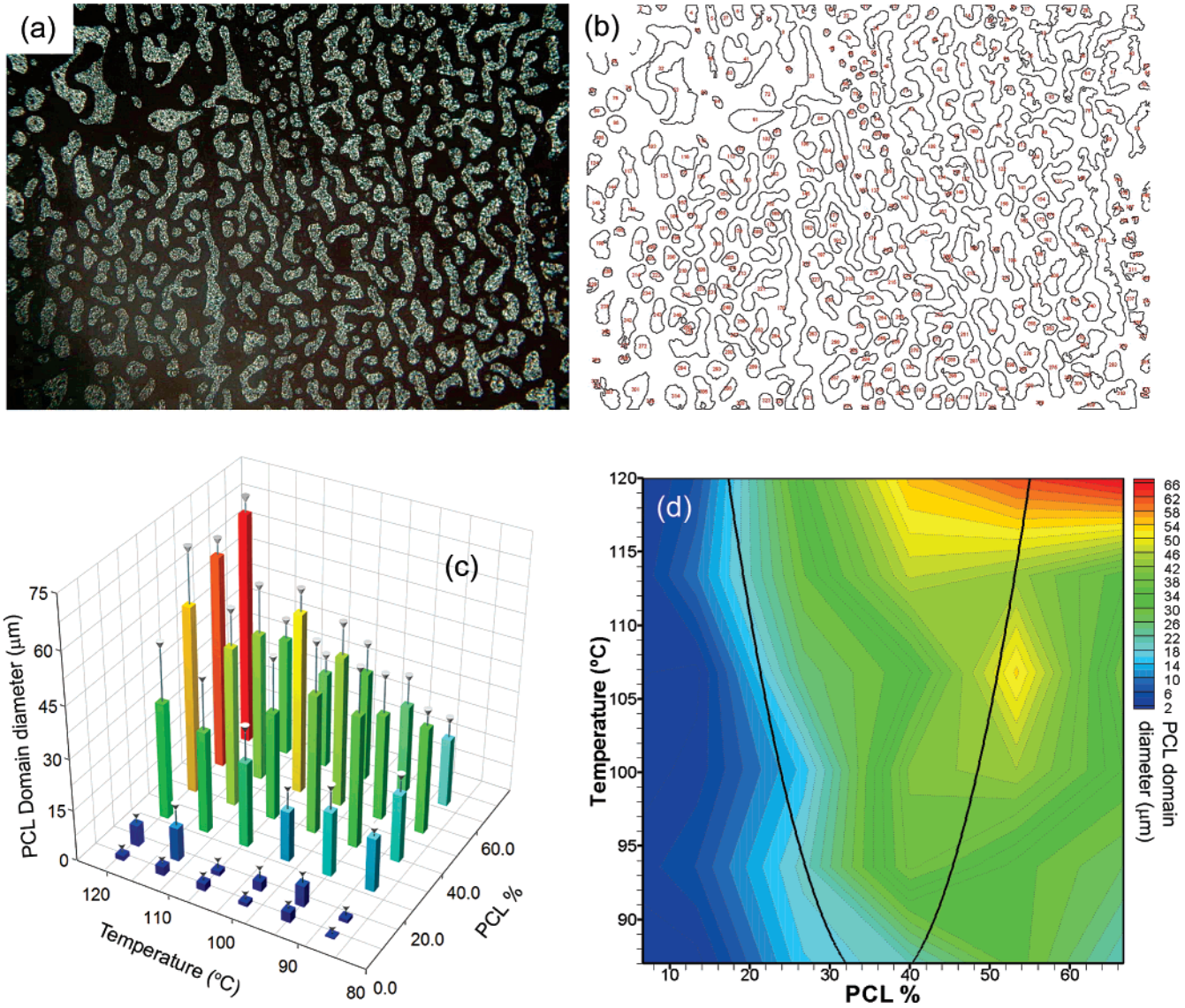


**Figure 3.** Library microstructure size characterization. (a) Microstructure morphology of a phase-separated PCL/PDLA polymer blend: Polarized optical micrograph. Bright and dark regions correspond to crystalline PCL and amorphous PDLA, respectively. Image size is 500 $\mu$m × 330 $\mu$m. (b) Outlines of the measured regions generated during the image analysis procedure. (c) PCL domain Feret's diameter profile across a temperature-annealed PCL/PDLA composition-gradient library. Values presented as averages ± SEM (indicated by error bars delimited by inverted cone markers, $n = 4$ replicates). (d) Average contour map of the PCL domain Feret's diameter values over the composition-gradient library. The solid curve represents the LCST cloud point boundary.

Probes, Inc.). Optimal dye concentrations were found to be 1.8 $\mu$M calcein AM and 3.6 $\mu$M EthD-1 for TCPS positive controls and 2.1 $\mu$M calcein AM and 4.2 $\mu$M EthD-1 for PCL/PDLA libraries. Samples were incubated for 45 min at room temperature after being concurrently stained with calcein AM and EthD-1. Quantification of cell viability was completed by fluorescence microscopy and image analysis. Cell viability assays were performed in parallel, in separate libraries, with the attachment/spreading, and proliferation tests.

**2.7. Statistical Analysis.** Data for the cell density assay was analyzed by two-way analysis of variance (ANOVA); $p < 0.05$ was defined as significant. The Tukey post hoc test was used for pairwise comparisons of significant factors. All results are expressed as mean ± standard error of the mean (SEM).

## 3. Results and Discussion

**3.1. Library Characterization.** While measurements demonstrating the linear composition gradients in polymer blend libraries have been presented previously,[41,42] we include here an investigation of the effects of thermal annealing on the gradient. It is possible that diffusion during annealing above the glass transition temperature would lead to significant distortion of the gradient and mistaken identification of composition during later screening. PCL compositions ($\phi_{PCL}$) before annealing, obtained by area integration of the PCL signature peak in the $CH_2$ symmetric stretch regime of the FTIR spectra ($\nu = 2864$ cm$^{-1}$, Supporting Information Figure 1) and direct comparison with a calibration (Materials and Methods) (Figure 1), show good agreement with the linear profile predicted from a mass balance model of the preparation process (model shown elsewhere[41]). A diffusion length ($\sqrt{Dt}$) of approximately 849 nm (equivalent to 0.0035% of the library width) suggests minimal diffusion influence during the 2 h library annealing step on the composition-gradient integrity. This was corroborated with PCL compositions measured on the same libraries after annealing at $T = 100$ °C (Figure 1). The PCL composition

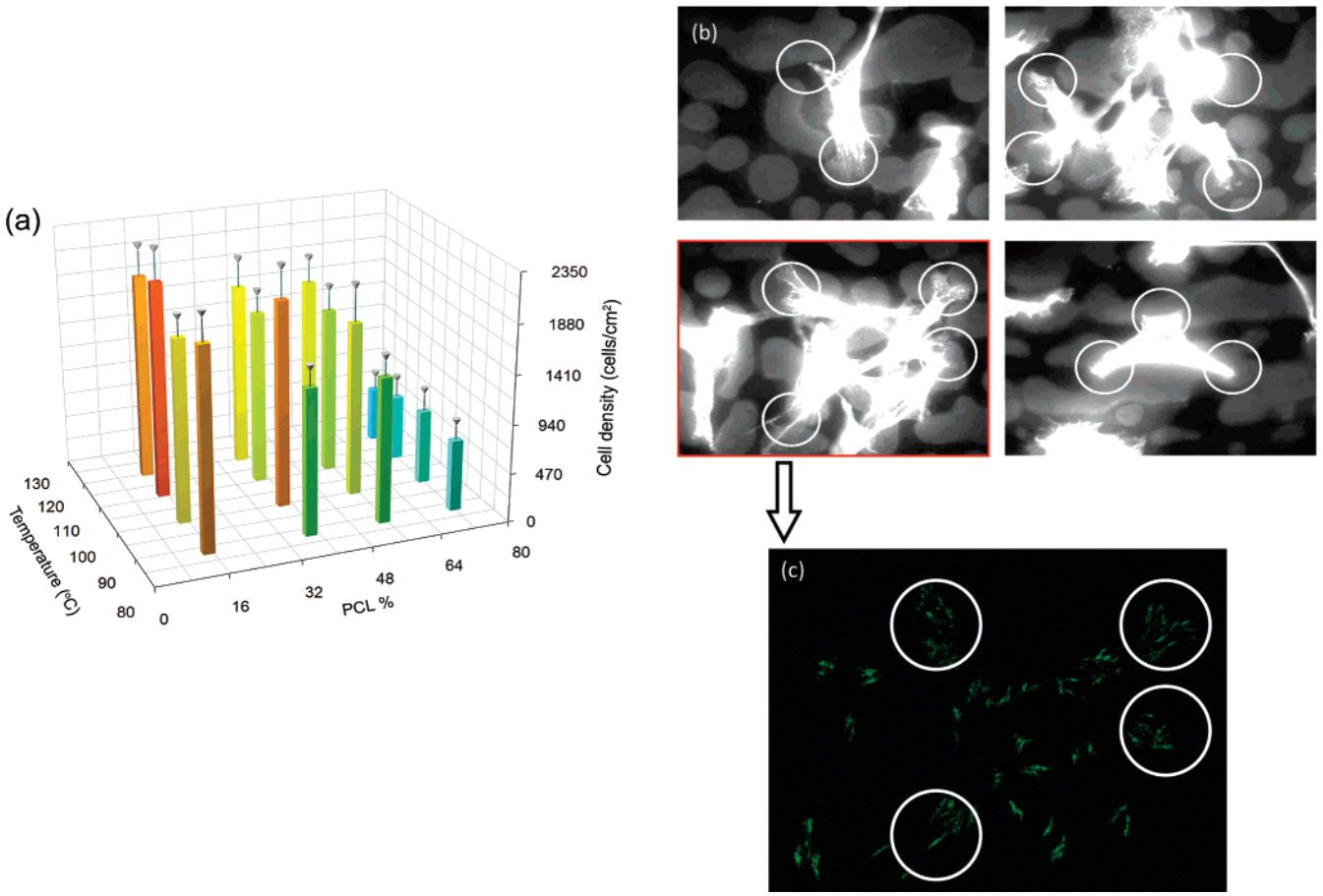


**Figure 4.** (a) MC3T3-E1 attachment density over PCL/PDLA combinatorial libraries after a 6 h culture period. Values presented as averages ± SEM ($n = 5$ replicates). (b) Overexposed fluorescent images (530−560 nm excitation wavelength) of rhodamine phalloidin-stained MC3T3-E1 osteoblasts adhered on different locations inside the phase-separated regime of combinatorial PCL/PDLA libraries. Brighter and darker background structures correspond to PDLA-rich and PCL-rich domains, respectively. Highlighted areas show cell attachment points onto PDLA-rich areas. (c) Fluorescence images under green filter from the same image as the lower-left in panel b, indicating vinculin staining. Vinculin accumulations are found predominantly on PDLA regions, typical of results found on the entire library.

profile after annealing was statistically indistinguishable from that before annealing.

A general trend of increased surface roughness with annealing temperature was evident throughout the entire composition range (Figure 2). Roughness passed through a maximum value as a function of PCL composition at constant temperature. Surface roughness ranged from approximately 5 to 255 nm, being markedly augmented in the upper $T$ and $\phi_{PCL}$ regions of the LCST regime ($T \cong 114$ °C and $\phi_{PCL} \cong 0.5$). The noticeable increase in surface roughness deep inside the LCST regime and gradual decrease toward the LCST limits is representative of the micropatterned structures formed during polymer demixing.

Image analysis of cross-polarized optical micrographs of the annealed libraries (Figure 3) revealed a continuous increase of PCL-rich domain size (Feret's diameter) with increasing anneal $T$ inside the phase-separated regime. The domain size is a complex function of the free energy of mixing of the polymers, the blend stability (bimodal vs spinodal behavior), and the kinetics of nucleation and growth. Response of microstructure size to composition variations presented a similar trend to that of surface roughness. PCL-rich domain size initially increased as PCL mass fraction entered the LCST region. As PCL composition increases inside the LCST, a maximum PCL diameter is reached, indicating phase inversion to a demixed blend with cocontinuous or continuous PCL with PDLA-rich domains. The average Feret's diameter of PCL-rich regions encompassed a range of approximately $0.5\ \mu m < d_{PCL} < 70\ \mu m$, covering a wide span above and below the MC3T3-E1 osteoblast mean size.

It should be noted that the locus of the LCST cloud point curve shown in Figures 2b and 3d is an approximation of the true thermodynamic phase boundary. Kinetic effects due to varying heating and cooling rates during annealing, dissimilar phase separation rates between nucleation and growth and spinodal decomposition near critical composition regions, and anisotropy induced by the film coating process are some of the factors that can generate moderate shifts of the phase boundary. These factors may contribute to demixed domains that extend to regions just outside of the "expected" LCST cloud point curve.

**3.2. Cell Attachment and Morphology.** Initial osteoblast attachment density to combinatorial libraries after a 6 h culture is shown in Figure 4a. The number of adherent cells per unit area was significantly greater on areas of moderate to low PCL concentration ($\phi_{PCL} \leq 0.35$), reaching the highest cell density levels (~2100 cells/cm$^2$) close to $\phi_{PCL} = 0.15$. This was comparable to an average cell density of 2030 ± 90 cells/cm$^2$ observed on "positive" TCPS controls. At $\phi_{PCL}$ below 0.15 cells adhered nearly uniformly along lines of constant composition inside *and* outside the LCST boundary, regardless of the varying surface morphology generated by the annealing temperature gradient. Moreover, cell density was low (~600 cells/cm$^2$) in the PCL-rich region ($\phi_{PCL} \geq 0.71$). Measurements of surface wettability of PCL and PDLA showed average contact angles

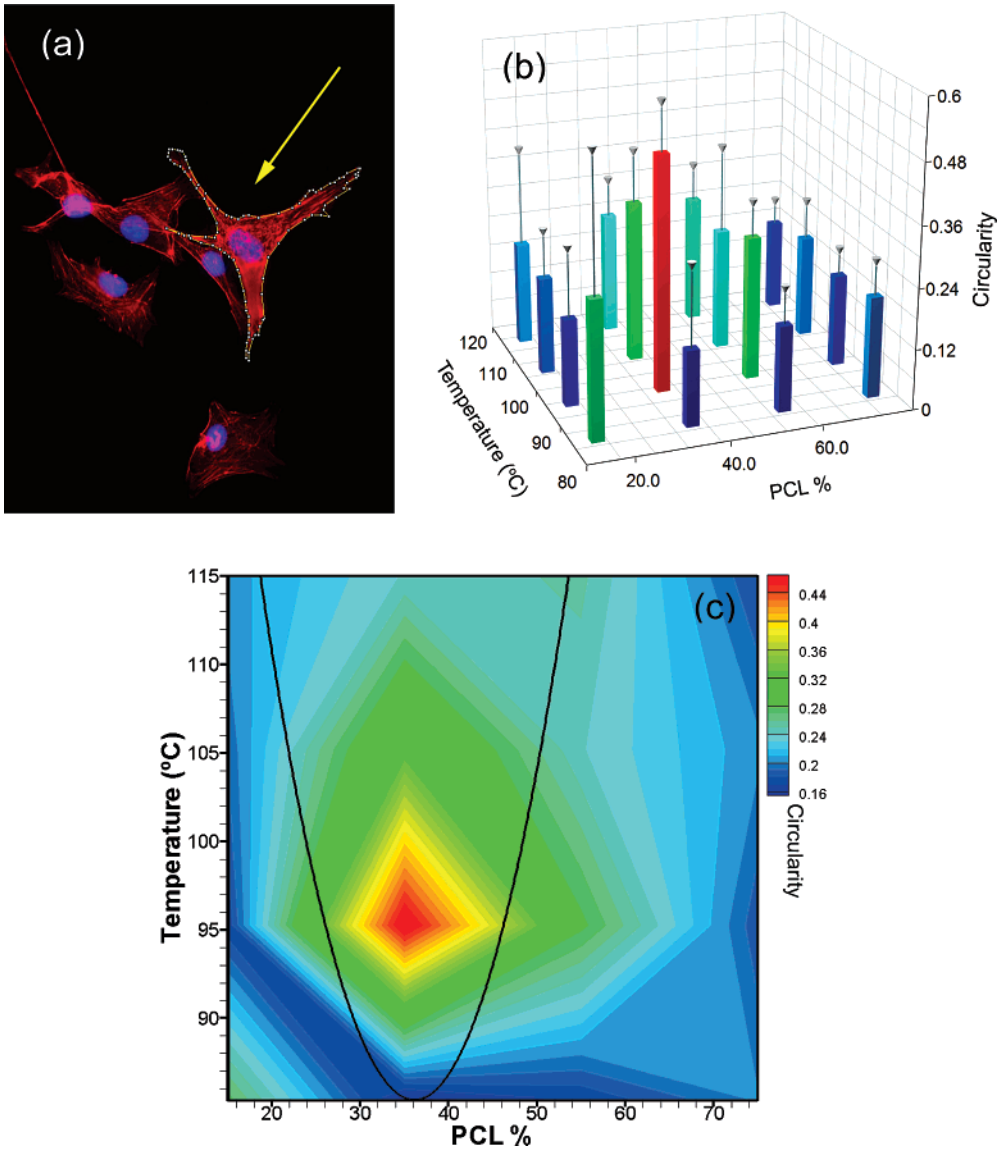


**Figure 5.** (a) Cell boundary identification by adaptive edge detection for circularity analysis. (b) Circularity of MC3T3-E1 cells cultured over PCL/PDLA combinatorial libraries for 6 h. Values presented as averages ± SEM (represented by inverted cone marker error bars, $n = 5$ replicates). (c) Contour map of average circularity values. Solid line represents the PCL/PDLA LCST cloud point.

of 60.4° ± 0.4° and 78.5° ± 0.8° for pure PDLA and pure PCL, respectively, suggesting that cells attach preferentially to higher surface energy PDLA regions (more hydrophilic). Consistent with this result, no significant effects of temperature (significance level $p = 0.62$) or combined temperature/composition effects ($p = 0.73$) were detected, leaving the composition effect as the only statistically significant factor ($p < 0.01$) that influenced initial cell adherence over the libraries.

Differences in PCL and PDLA autofluorescence when overexposed (12−15 s excitation, 8× gain) using a 530−560 nm excitation source helped corroborate the aforementioned results. High-magnification (600×) *overexposed* fluorescent images of rhodamine phalloidin-stained MC3T3-E1 osteoblasts inside the demixed zone revealed that cells are stretched between attachment sites on the PDLA-rich domains, (Figure 4b). Vinculin counterstaining (via normal exposure) indicated that the highest densities of vinculin were located on the PDLA islands on the overexposed images (Figure 4c).

While cells presented pleomorphic forms all over the libraries, spreading and cytoskeletal rearrangement showed a marked dependence on physical surface features. Spread multipolar morphologies, characterized by numerous highly organized F-actin stress fibers and high cell area, were predominant on the rougher regions of the LCST regime. Bipolar, spindle-shaped cells characterized by reduced cell area and minimal F-actin stress fibers were predominant outside the two-phase region (Supporting Information Figure 2). A cell circularity factor was used to quantify cell spreading as a function of composition and process temperature. Circularity is relatively sensitive to "branched" morphologies (i.e., multipolar mammalian cells), allowing one to account for spreading levels and cell shape. Circularity values approaching 0 indicate increasingly elongated profiles, while a value of 1 indicates a perfect circle. Well-spread cells, however, normally present polygonal processes that give them a stellate aspect rather than a circular shape and, hence, present reduced circularity. The circularity of well-spread stellate morphologies of MC3T3-E1 cells over TCPS ranges between $0.4 < C < 0.6$. Bipolar-shaped cells that are less well-spread present circularity values between $0.08 < C < 0.2$, which is typical of MC3T3 attached to surfaces treated with hydrophobic plasma deposited polymers, neutral hydrophilic hydrogels, or amine and methyl silane-treated surfaces.[48]

Circularity was measured by adaptive cell boundary detection image analysis (Materials and Methods) (Figure 5a). Measure-

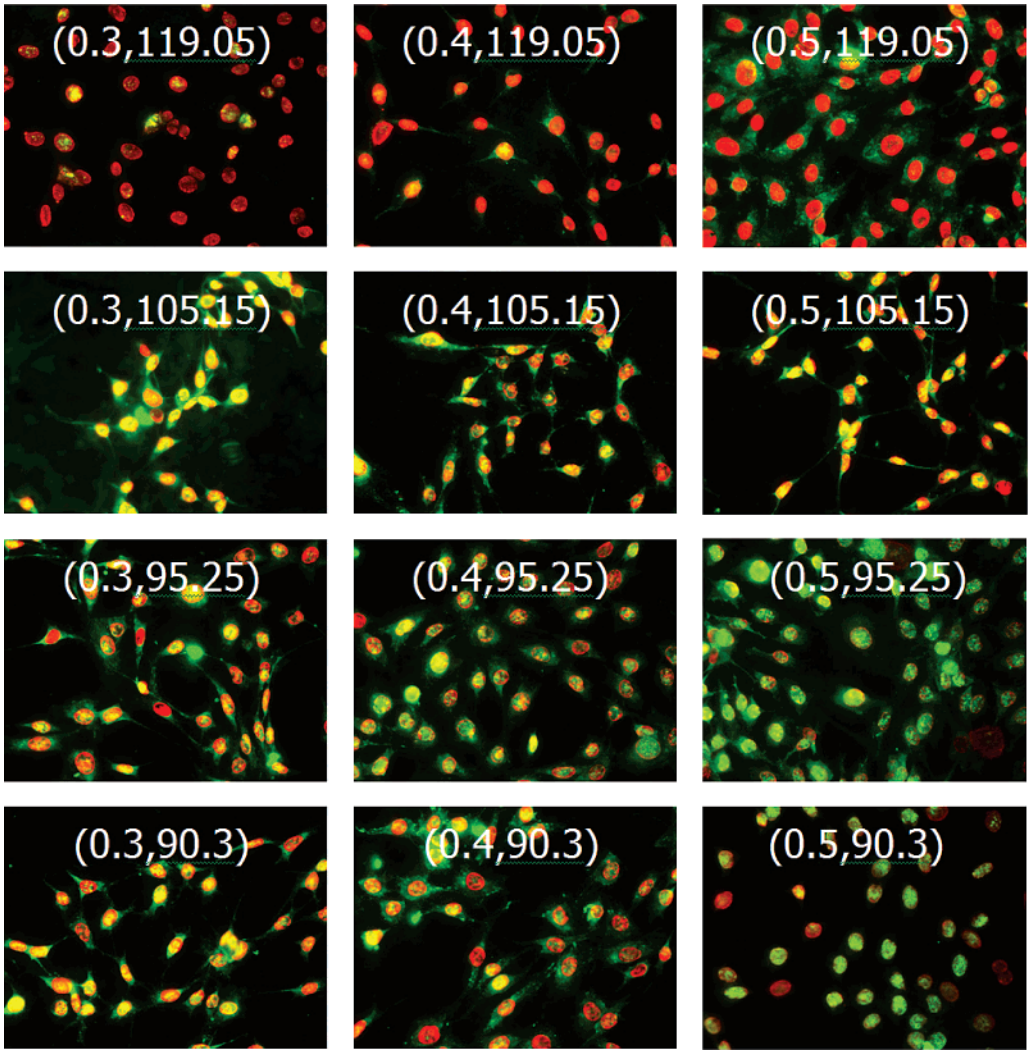


**Figure 6.** Immunofluorescence staining for proliferation of MC3T3-E1 osteoblasts over a PCL/PDLA combinatorial library after a 3 day culture. Cells were stained with Alexa Fluor 488 (green) for BrdU incorporated into proliferated cells and counterstained with EthD-2 (red) to quantify the total number of cells. Numbers in parenthesis indicate PCL mass fraction and temperature in °C, respectively. Cell passage number was 5.

ments performed over five distinct libraries show a clear cell spreading enhancement in the LCST regime compared to the one-phase region (Figure 5, parts b and c). However, this increase in cell spreading was not general to the entire demixed portion of the library as circularity was particularly high ($0.40 < C < 0.47$) toward the center (area comprised between 95 °C $< T <$ 100 °C and $0.3 < \phi_{PCL} < 0.4$), and a gradual decline was noticed toward the upper and lower areas (high- and low-temperature regions of the LCST regime), where circularity reached values as low as 0.24 and 0.16, respectively.

The preferential adhesion of MC3T3-E1 osteoblasts to more hydrophilic PDLA-rich domains and the influence of surface microstructures and topography on cell morphology and cytoskeletal organization suggest that there is an optimal polymer demixing level (lateral pattern size and surface roughness distribution) that promotes cell spreading. Based on the response of the cytoskeleton to stress conditions imposed by the underlying substrate witnessed in other cell lines,[20,22,49] we hypothesize that internal stress generated when cells stretch over PCL domains promotes multipolar spreading and production of F-actin stress fibers. In fact, the region between 95 °C $< T <$ 100 °C and $0.3 < \phi_{PCL} < 0.4$, corresponding to PCL-rich diameters of 20 $\mu$m $< d_{PCL} <$ 40 $\mu$m and roughnesses of 113 nm $< R_{RMS} <$ 177 nm, exhibited 17−37% improved cell spreading (circularity range $0.4 < C < 0.47$) when compared to that of TCPS standards (average circularity for TCPS controls was $0.34 \pm 0.09$) (Figure 5b).

**3.3. Cell Proliferation.** Figure 6 displays an arrangement of fluorescent micrographs of multiple locations over a BrdU and EthD-2 stained library after a 3 day culture, revealing the existence of marked differences in proliferation levels as a function of process temperature and composition. For example, MC3T3-E1 proliferation was higher in the lower portion of the library ($\phi_{PCL} = 0.5$ and 90.3 °C $< T <$ 95.2 °C). Proper quantification of the cell proliferation ratio (proliferated cells to total number of cells) over the libraries was performed via image analysis. Results are shown in Figure 7a−d.

An interesting trend in MC3T3-E1 proliferation was observed after 3 days in culture (Figure 7a); cells have a higher proliferation ratio ($0.88 \pm 0.18$) near the lower limit of the LCST phase-separated region ($0.47 < \phi_{PCL} < 0.51$ and 90 °C $< T <$ 94 °C). This region, characterized by small to medium diameter PCL domains (approximately 21 $\mu$m $< d_{PCL} <$ 33 $\mu$m) and moderate roughness (85 nm $< R_{RMS} <$ 105 nm), presented remarkably poor cell spreading and cytoskeletal organization upon initial attachment ($0.18 < C < 0.28$). The results suggest that the enhanced spreading (Figure 5c) in the mid-to-lower part of the LCST (resulting from cell stretching between PDLA-rich domains) is not necessarily beneficial for cell proliferation. A possible explanation for this behavior can be nonuniform

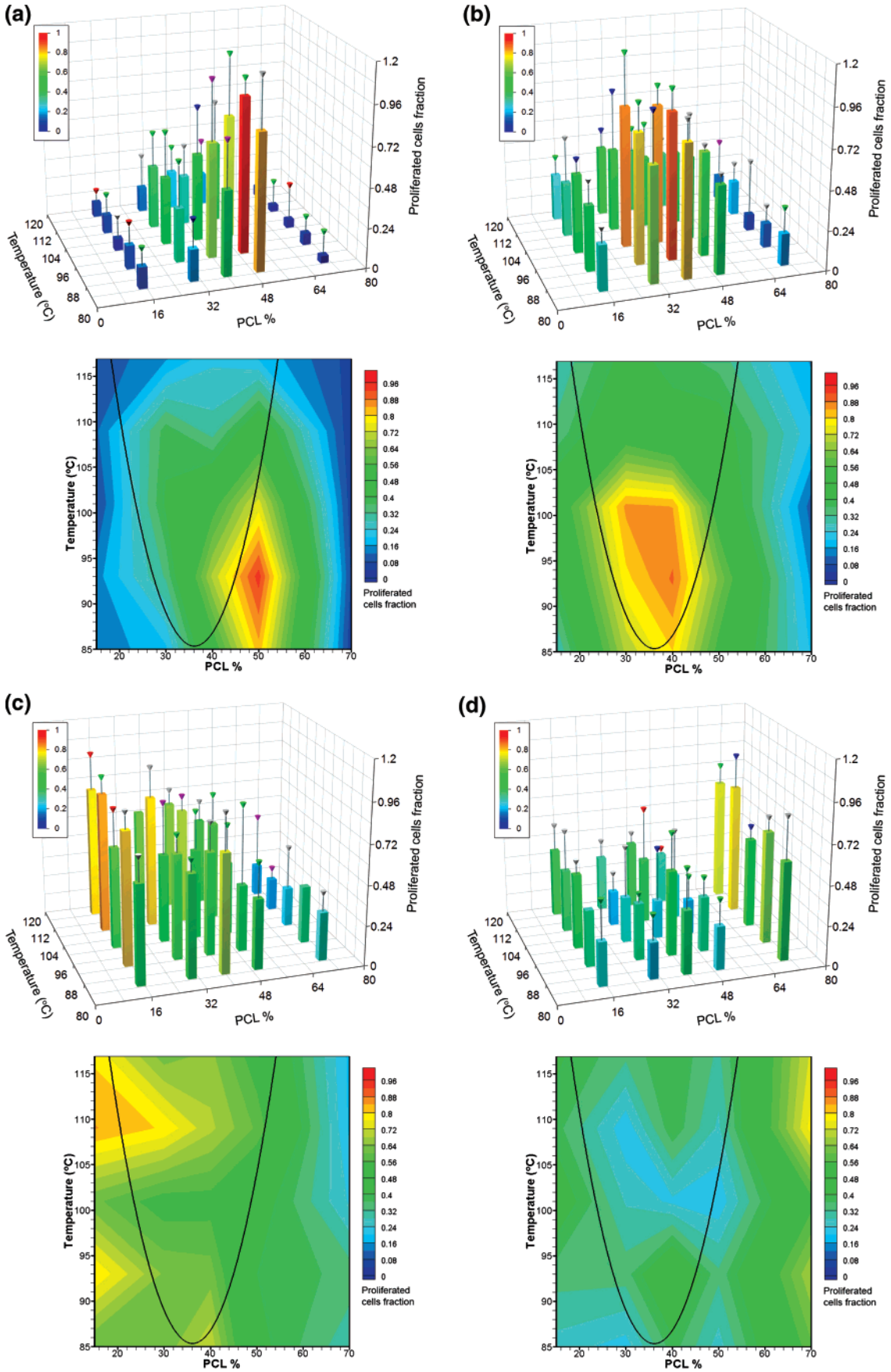


**Figure 7.** Proliferated to total number of MC3T3-E1 cells ratio over a combinatorial PCL/PDLA library as a function of temperature and composition after (a) 3 day culture (cell passage 5), (b) 4 day culture (cell passage 7), (c) 5 day culture (cell passage 4), (d) 8 day culture (cell passage 4). Top images: Values presented as averages ± SEM. The number of replicates for each measurement is given by the color of the inverted cone markers at the end of the error bars: $n = 6$ blue mark, $n = 5$ gray mark, $n = 4$ green mark, $n = 3$ violet mark, $n = 2$ red mark, $n = 1$ no mark. Bottom images: Average proliferation ratio contour map showing the PCL/PDLA LCST phase boundary.

tension in the cytoskeleton of the well-spread morphologies attained inside the LCST regime. Nonuniform tension has been reported to delay, or even inhibit, the progression of the G1 phase of the cell cycle, resulting in a restriction of cell proliferation.[14] Notice also that recent studies of MC3T3-E1 proliferation response to nanometer-scale surface roughness suggest the existence of a local, and material-dependent, critical roughness value above which proliferation is drastically reduced.[35] This behavior has been previously noticed for different cell lines. For example, proliferation of rat calvarial cells increased with roughness up to a point where further roughness rise led to decreased cell proliferation.[17] This may be related to the fact that the S phase of the cell cycle can only proceed when cells are spread to an *appropriate* degree.[50]

After 4 days in culture (Figure 7b) the high MC3T3-E1 proliferation regime (proliferation ratio $0.84 \pm 0.15$) shifted to the lower portion inside the two-phase region ($0.35 < \phi_{PCL} < 0.42$ and $91\ °C < T < 97\ °C$). A small increase in cell proliferation was also observed in the high PDLA concentration region (left portion outside the LCST regime, $0 < \phi_{PCL} < 0.3$) as well as the upper part of the LCST regime. The high PCL concentration region, on the other hand, followed the tendency seen after a 3 day culture in the same region, showing marginal proliferation levels ($0.16 \pm 0.14$). There was also a reduction in proliferation ($0.56 \pm 0.09$) in the area with the highest levels of cell replication for the 3 day assay, which seems to be in agreement with the downregulation of proliferation as cell density increases prior to differentiation.

Results of the 5 day proliferation assay are shown in Figure 7c. At this point proliferation was prominent only in some areas of the high PDLA concentration region at the upper left portion of the LCST region ($0.18 < \phi_{PCL} < 0.26$ and $109\ °C < T < 114\ °C$), where the proliferation ratio was approximately $0.72 \pm 0.16$. The rest of the library, with the exception of the high PCL concentration domain, seemed to be leveling and lowering the cell replication rate as cells were almost confluent (proliferation ratio ~0.4). The effect of the diverse topographies across the library on cell proliferation is seen easily by following the maximum proliferation positions at each time point: the LCST transition region with low roughness and moderate to small microstructures just outside the LCST regime at day 3, middle and lower parts of the two-phase regime at day 4, and upper parts of the phase-separated region at day 5.

The 8 day assay (Figure 7d) showed an upsurge in the proliferation ratio ($0.66 \pm 0.12$) at high concentrations of PCL. This increase in cell growth in the most hydrophobic area of the library, after a prolonged cell culture, suggests that cell proliferation is retarded by low-energy substrata. On the other hand, the rest of the library was almost confluent and exhibited signs of strong downregulation of proliferation, which is characteristic of the onset of differentiation, although assays for differentiation were not performed in this study. After 13 days (data not shown) proliferation leveled out and the entire surface of each library was confluent (proliferation ratio ~0.09). Only negligible cell growth activity was witnessed at randomly chosen locations, suggesting a microstructure-independent inhibition of proliferation.

Cell viability ranged between 98.5% and 100% throughout the entire library surface, and no significant viability differences among library compositions were observed. (Data not shown.)

On the whole we observed that cell response to PCL/PDLA surfaces is distinctly influenced by the polymer blend processing conditions. The effect of particular temperature−composition regimes on the libraries was found to vary with the cell event being evaluated. A summary of these "active" parameter combinations, including with the optimal PCL/PDLA properties (i.e., processing and physical) for each cell assay, is presented in Table 1. While composition is the only significant *preparatory* variable with respect to cell attachment (6 h adhesion), other properties such as proliferation and shape were dependent on both composition and annealing temperature. The nature of the combinatorial library design allows large numbers of parameter combinations to be screened rapidly under identical culture conditions. One can thus identify microstructures that are associated with the "active" versus "inactive" compositions and temperatures. However, this advantage in breadth prevents the identification of cause-and-effect with respect to the material *microstructure*. For example, composition and temperature both influence the number and size of PCL domains, the phase morphology, surface roughness, and hydrophilicity. Since these are varied simultaneously, it is difficult to identify a cause-and-effect relationship about the role of microstructure on cell response. The value offered by high-throughput cell−biomaterial screening is the ability to identify anomalous behavior and to sort important versus unimportant combinations of material factors rapidly and efficiently.

**Table 1.** Preparatory Conditions and Physical Characteristics of PCL/PDLA Blends That Exhibited Enhanced MC3T3-E1 Cellular Response

| assay | $\phi_{PCL}$ | $T$ (°C) | $d_{PCL}$ ($\mu$m) | $R_{RMS}$ (nm) |
|---|---|---|---|---|
| 6 h adhesion | 0−0.35 | | | |
| shape (6 h spreading) | 0.30−0.40 | 95−100 | 20−40 | 113−177 |
| 3 day proliferation | 0.47−0.51 | 90−94 | 21−33 | 85−105 |
| 4 day proliferation | 0.35−0.42 | 91−97 | 14−32 | 123−164 |
| 5 day proliferation | 0.18−0.26 | 109−114 | 11−20 | 68−96 |
| 8 day proliferation | 0.61−0.70 | | | |
| alkaline phosphatase[a] | 0.40−0.55 | 96−110 | 30 − 40[b] | 370 ± 50 |

[a] Ref 26. [b] The PCL island size in the previous work by Meredith et al. (ref 26) is given as the equivalent diameter (diameter of a circle with the same area of the island being measured). The actual study uses the maximal Feret's diameter as the PCL characteristic dimension since it is more appropriate for nonregular shapes, such as phase-separated microstructures.

## 4. Conclusions

Combinatorial libraries were used to screen the effects of preparatory conditions (temperature and composition) of complex, multifeature patterned surfaces on osteoblast biological responses. The microstructural patterns were created by phase separation of two biodegradable polyesters, PCL and PDLA. We observed that certain combinations of temperature and composition for the PCL/PDLA blends led to enhanced cell functions. These "active" conditions differed depending on the cell function assayed as well as with culture time. For example, the region ($\phi$, $T$) of maximum proliferation ratio changed depending on the day at which the assay was performed. By day 8 temperature no longer had a significant effect on proliferation. Cell adhesion at 6 h was a significant function only of the composition, but cell circularity was a function of both $T$ and $\phi$. Cell viability, on the other hand, did not depend significantly on composition or temperature at any time point assayed.

High-throughput screening may be viewed as an *applied* tool for engineering biomaterial surfaces to target a particular cell event and elicit a desired response for therapeutic applications. Screening also can play an important role in *fundamental* studies of cell−surface interaction. High-throughput screening experiments were successful in identifying the sample *preparation* conditions (composition, temperature) that should be included

in a detailed confirmatory experiment. It is likely that a combination of chemistry and physical surface features (height, droplet size, shape, spacing) works to enhance or suppress functions of adherent cells. The dependence of microstructure and roughness on both composition and temperature prevented a cause-and-effect conclusion regarding the controlling surface feature. However, the specific combination of microstructure and roughness at the "active" compositions and temperatures are known from the library. This information is crucial in designing an experiment to vary these effects independently. This challenge is the subject of forthcoming work.

**Acknowledgment.** The authors thank B. G. Keselowsky, J. R. Capadona, and K. E. Michael for helpful discussions and experimental assistance and NIH (RR17425 and HK072039) for providing funds for this work.

**Supporting Information Available.** FTIR spectra of a nonannealed PCL/PDLA continuous composition-gradient library and cytoskeleton organization and predominant morphologies of MC3T3-E1 immature osteoblasts at different composition/temperature regimes over PCL/PDLA combinatorial libraries. This material is available free of charge via the Internet at http://pubs.acs.org.

## References and Notes

(1) Castner, D. G.; Ratner, B. D. Biomedical surface science: Foundations to frontiers. *Surf. Sci.* **2002**, *500*, 28−60.
(2) Keselowsky, B. G.; Collard, D. M.; García, A. J. Surface chemistry modulates focal adhesion composition and signaling through changes in integrin binding. *Biomaterials* **2004**, *25*, 5947−5954.
(3) Keselowsky, B. G.; Collard, D. M.; García, A. J. Integrin binding specificity regulates biomaterial surface chemistry effects on cell differentiation. *Proc. Natl. Acad. Sci. U.S.A.* **2005**, *102* (17), 5953−5957.
(4) Keselowsky, B. G.; García, A. J. Quantitative methods for analysis of integrin binding and focal adhesion formation on biomaterial surfaces. *Biomaterials* **2005**, *26*, 413−418.
(5) Lan, M. A.; Gersbach, C. A.; Michael, K. E.; Keselowsky, B. G.; García, A. J. Myoblast proliferation and differentiation on fibronectin-coated self assembled monolayers presenting different surface chemistries. *Biomaterials* **2005**, *26*, 4523−4531.
(6) Curtis, A.; Riehle, M. O. Tissue engineering: The biophysical background. *Phys. Med. Biol.* **2001**, *46*, R47−R65.
(7) Brocchini, S.; James, K.; Tangpasuthadol, V.; Kohn, J. Structure−property correlations in a combinatorial library of degradable materials. *J. Biomed. Mater. Res.* **1998**, *42*, 66−75.
(8) Yang, X. B.; Roach, H. I.; Clarke, N. M. P.; Howdle, S. M.; Quirk, R.; Shakesheff, K. M.; Oreffo, R. O. C. Human osteoprogenitor growth and differentiation on synthetic biodegradable structures after surface modification. *Bone* **2001**, *29* (6), 523−531.
(9) Chung, T. W.; Lu, Y. F.; Wang, S. S.; Lin, Y. S.; Chu, S. H. Growth of human endothelial cells on photochemically grafted Gly-Arg-Gly-Asp (GRGD) chitosans. *Biomaterials* **2002**, *23*, 4803−4809.
(10) Hamerli, P.; Weigel, T.; Groth, T.; Paul, D. Surface properties and cell adhesion onto allylamine-plasma-coated polyethylenterephtalat membranes. *Biomaterials* **2003**, *24*, 3989−3999.
(11) Manwaring, M. E.; Biran, R.; Tresco, P. A. Characterization of rat meningeal cultures on materials of differing surface chemistry. *Biomaterials* **2001**, *22*, 3155−3168.
(12) Thomas, C. H.; Collier, J. H.; Sfeir, C. S.; Healy, K. E. Engineering gene expression and protein synthesis by modulation of nuclear shape. *Proc. Natl. Acad. Sci. U.S.A.* **2002**, *99*, 1972−1977.
(13) Huang, S.; Ingber, D. E. Shape-dependent control of cell growth, differentiation, and apoptosis: Switching between attractors in cell regulatory networks. *Exp. Cell Res.* **2000**, *261*, 91−103.
(14) Huang, S.; Chen, C. S.; Ingber, D. E. Control of cyclin D1, $p27^{Kip1}$, and cell cycle progression in human capillary endothelial cells by cell shape and cytoskeletal tension. *Mol. Biol. Cell* **1998**, *9*, 3179−3193.
(15) Lampin, M.; Warocquier-Clerout, R.; Legris, C.; Degrange, M.; Sigot-Luizard, M. F. Correlation between substratum roughness and wettability, cell adhesion, and cell migration. *J. Biomed. Mater. Res.* **1997**, *36*, 99−108.
(16) Miller, C.; Shanks, H.; Witt, A.; Rutkowski, G.; Mallapragada, S. Oriented Schwann cell growth on micropatterned biodegradable polymer substrates. *Biomaterials* **2001**, *22*, 1263−1269.
(17) Hatano, K.; Inoue, H.; Kojo, T.; Matsunaga, T.; Tsujisawa, T.; Uchiyama, C.; Uchida, Y. Effect of surface roughness on proliferation and alkaline phosphatase expression of rat calvarial cells cultured on polystyrene. *Bone* **1999**, *25* (4), 439−445.
(18) Schwartz, Z.; Lohmann, C. H.; Vocke, A. K.; Sylvia, V. L.; Cochran, D. L.; Dean, D. D.; Boyan, B. D. Osteoblast response to titanium surface roughness and 1α,25-(OH)2D3 is mediated through the mitogen-activated protein kinase (MAPK) pathway. *J. Biomed. Mater. Res.* **2001**, *56*, 417−426.
(19) Soboyejo, W. O.; Nemetski, B.; Allameh, S.; Marcantonio, N.; Mercer, C.; Ricci, J. Interactions between MC3T3-E1 cells and textured Ti6Al4V surfaces. *J. Biomed. Mater. Res.* **2002**, *62*, 56−72.
(20) Dalby, M. J.; Childs, S.; Riehle, M. O.; Johnstone, H. J. H.; Affrossman, S.; Curtis, A. S. G. Fibroblast reaction to island topography: Changes in cytoskeleton and morphology with time. *Biomaterials* **2003**, *24*, 927−935.
(21) Dalby, M. J.; Riehle, M. O.; Johnstone, H. J. H.; Affrossman, S.; Curtis, A. S. G. In vitro reaction of endothelial cells to polymer demixed nanotopography. *Biomaterials* **2002**, *23*, 2945−2954.
(22) Dalby, M. J.; Yarwood, S. J.; Riehle, M. O.; Johnstone, H. J. H.; Affrossman, S.; Curtis, A. S. G. Increasing fibroblast response to materials using nanotopograhy: Morphological and genetic measurements of cell response to 13-nm-high polymer demixed islands. *Exp. Cell Res.* **2002**, *276*, 1−9.
(23) Brocchini, S.; James, K.; Tangpasuthadol, V.; Kohn, J. Structure−property correlations in a combinatorial library of degradable biomaterials. *J. Biomed. Mater. Res.* **1998**, *42* (1), 66−75.
(24) Hoogenboom, R.; Meier, M. A. R.; Schubert, U. S. Combinatorial methods, automated synthesis and high-throughput screening in polymer research: Past and present. *Macromol. Rapid Commun.* **2003**, *24*, 15−32.
(25) Amis, E. J.; Xiang, X.-D.; Zhao, J.-C. Combinatorial materials science: What's new since Edison? *MRS Bull.* **2002**, *27* (4), 295−296.
(26) Meredith, J. C.; Sormana, J. L.; Keselowsky, B. G.; García, A. J.; Tona, A.; Karim, A.; Amis, E. J. Combinatorial characterization of cell interactions with polymer surfaces. *J. Biomed. Mater. Res.* **2003**, *66A*, 483−490.
(27) Kennedy, S.; Washburn, N.; Sehgal, A.; Karim, A.; Amis, E. Combinatorial assay of cells on topographically patterned surfaces. *Abstr. Pap.—Am. Chem. Soc.* **2002**, *224*, U237.
(28) Smith, J.; Seyda, A.; Weber, N.; Knight, D.; Abramson, S.; Kohn, J. Integration of combinatorial synthesis, rapid screening, and computational modeling in biomaterials development. *Macromol. Rapid Commun.* **2004**, *25*, 127−140.
(29) Washburn, N.; Simon, C.; Weir, M.; Bailey, L.; Kennedy, S.; Amis, E. Combinatorial screen of cell−material interactions. *Abstr. Pap.—Am. Chem. Soc.* **2004**, *227*, U557.
(30) Simon, C. G.; Eidelman, N.; Kennedy, S. B.; Sehgal, A.; Khatri, C. A.; Washburn, N. R. Combinatorial screening of cell proliferation on poly(L-lactic acid)/poly(D,L-lactic acid) blends. *Biomaterials* **2005**, *26*, 6906−6915.
(31) Kennedy, S.; Washburn, N.; Simon, C.; Amis, E. Combinatorial screen of the effect of surface energy on fibronectin-mediated osteoblast adhesion, spreading and proliferation. *Biomaterials* **2006**, *27*, 3817−3824.
(32) Petro, M.; Nguyen, S. H.; Liu, M.; Kolosov, O. Combinatorial exploration of polymeric transport agents for targeted delivery of bioactives to human tissues. *Macromol. Rapid Commun.* **2004**, *25*, 178−188.
(33) Akinc, A.; Lynn, D. M.; Anderson, D. G.; Langer, R. Parallel synthesis and biophysical characterization of a degradable polymer library for gene delivery. *J. Am. Chem. Soc.* **2003**, *125*, 5316−5323.
(34) Anderson, D. G.; Putnam, D.; Lavik, E. B.; Mahmood, T. A.; Langer, R. Biomaterial microarrays: rapid, microscale screening of polymer−cell interaction. *Biomaterials*, in press.
(35) Washburn, N. R.; Yamada, K. M.; Simon, C. G., Jr.; Kennedy, S. B.; Amis, E. J. High-throughput investigation of osteoblast response to polymer crystallinity: influence of nanometer-scale roughness on proliferation. *Biomaterials* **2004**, *25*, 1215−1224.
(36) Meredith, J. C. A perspective on high-throughput polymer science. *J. Mater. Sci.* **2003**, *38* (22), 4427−4437.
(37) Engelberg, I.; Kohn, J. Physicomechanical properties of degradable polymers used in medical applications: A comparative study. *Biomaterials* **1991**, *12*, 292−304.

(38) Broz, M. E.; VanderHart, D. L.; Washburn, N. R. Structure and mechanical properties of poly(d,l-lactic acid)/poly(ϵ-caprolactone) blends. *Biomaterials* **2003**, *24*, 4181−4190.
(39) Meredith, J. C.; Amis, E. J. LCST phase separation in biodegradable polymer blends: poly(D,L-lactide) and poly(ϵ-caprolactone). *Macromol. Chem. Phys.* **2000**, *201* (6), 733−739.
(40) Meredith, J. C.; Smith, A. P.; Karim, A.; Amis, E. J. Combinatorial materials science for polymer thin-film dewetting. *Macromolecules* **2000**, *33*, 9747−9756.
(41) Meredith, J. C.; Karim, A.; Amis, E. J. High-throughput measurement of polymer blend phase behavior. *Macromolecules* **2000**, *33*, 5760−5762.
(42) Karim, A.; Sehgal, A.; Amis, E. J.; Meredith, J. C. Combinatorial mapping of polymer blends phase behavior. In *Experimental Design for Combinatorial and High Throughput Materials Development*; Cawse, J. N., Ed.; John Wiley & Sons, Inc.: Hoboken, NJ, 2003; pp 73−88.
(43) Kodama, H.; Amagai, Y.; Sudo, H.; Kasai, S.; Yamamoto, S. Establishment of a clonal osteogenic cell line from newborn mouse calvaria. *Jpn. J. Oral Biol.* **1981**, *23*, 899−901.
(44) Sudo, H.; Kodama, H.; Magai, Y.; Yamamoto, S.; Kasai, S. In vitro differentiation and calcification in a new clonal osteogenic cell line derived from newborn mouse calvaria. *J. Cell Biol.* **1983**, *96*, 191−198.
(45) Choi, J.; Lee, B.; Song, K.; Park, R.; Kim, I.; Sohn, K.; Jo, J.; Ryo, H. Expression patterns of bone-related proteins during osteoblastic differentiation in MC3T3-E1 cells. *J. Cell. Biochem.* **1996**, *61*, 609−618.
(46) Sodek, J.; Berkman, F. A. Bone cell cultures. *Methods Enzymol.* **1987**, *145*, 303−324.
(47) Gallant, N. D.; Michael, K. E.; García, A. J. Cell adhesion strengthening: Contributions of adhesive area, integrin binding, and focal adhesion assembly. *Mol. Biol. Cell* **2005**, *16*, 4329−4340.
(48) Webb, K.; Hlady, V.; Tresco, P. A. Relationships among cell attachment, spreading, cytoskeletal organization, and migration rate for anchorage-dependent cells on model surfaces. *J. Biomed. Mater. Res.* **2000**, *49*, 362−368.
(49) Girard, P. R.; Nerem, R. M. Shear stress modulates endothelial cell morphology and F-actin organization through the regulation of focal adhesion-associated proteins. *J. Cell. Physiol.* **1995**, *163*, 179−193.
(50) Folkman, J.; Moscona, A. Role of cell shape in growth control. *Nature* **1978**, *273*, 345−349.

BM061134T